The Astronomical Journal, 143:40 (15pp), 2012 February doi:10.1088/0004-6256/143/2/40

THE BARYONIC TULLY–FISHER RELATION OF GAS-RICH GALAXIES AS A TEST OF ΛCDM AND MOND

Stacy S. McGaugh
Department of Astronomy, University of Maryland College Park, MD 20742-2421, USA
Received 2010 December 6; accepted 2011 December 7; published 2012 January 12

ABSTRACT

The baryonic Tully–Fisher relation (BTFR) is an empirical relation between baryonic mass and rotation velocity in disk galaxies. It provides tests of galaxy formation models in ΛCDM and of alternative theories like modified Newtonian dynamics (MOND). Observations of gas-rich galaxies provide a measure of the slope and normalization of the BTFR that is more accurate (if less precise) than that provided by star-dominated spirals, as their masses are insensitive to the details of stellar population modeling. Recent independent data for such galaxies are consistent with $M_b = AV_f^4$ with $A = 47 \pm 6\,M_\odot\,\mathrm{km}^{-4}\,\mathrm{s}^4$. This is equivalent to MOND with $a_0 = 1.3 \pm 0.3$ Å s^{-2}. The scatter in the data is consistent with being due entirely to observational uncertainties. It is unclear why the physics of galaxy formation in ΛCDM happens to pick out the relation predicted by MOND. We introduce a feedback efficacy parameter $\mathcal{E}$ to relate halo properties to those of the galaxies they host. $\mathcal{E}$ correlates with star formation rate and gas fraction in the sense that galaxies that have experienced the least star formation have been most impacted by feedback.

Key words: galaxies: dwarf – galaxies: irregular – galaxies: kinematics and dynamics – galaxies: spiral

Online-only material: color figures

1. INTRODUCTION

The Tully–Fisher relation (Tully & Fisher 1977) is one of the strongest empirical correlations in extragalactic astronomy. In addition to being a useful distance indicator (e.g., Sakai et al. 2000), the physical basis of this relation is of fundamental importance. In the context of ΛCDM, the Tully–Fisher relation places tight constraints on galaxy formation models (e.g., Eisenstein & Loeb 1996; McGaugh & de Blok 1998a; Mo et al. 1998; Courteau & Rix 1999; Steinmetz & Navarro 1999; Courteau & Rix 1999; van den Bosch 2000; Bullock et al. 2001; Mo & Mao 2004; Mayer & Moore 2004; Gnedin et al. 2007; Governato et al. 2007; Trujillo-Gomez et al. 2011; de Rossi et al. 2010; Tonini et al. 2010). In a broader context, it provides a useful test of theories that seek to modify gravity in order to obviate the need for dark matter (e.g., Milgrom 1983; Sanders 1984; Mannheim & Kazanas 1989; Moffat 2006). These should make specific and testable predictions for the Tully–Fisher relation.

The Tully–Fisher relation was originally posed as an empirical relation between optical luminosity and the width of the 21 cm line. These are presumably proxies for more physical quantities. The 21 cm line width is a proxy for rotation velocity (e.g., Verheijen 2001; Yegorova & Salucci 2007), which is widely presumed to be set by the dark matter halo. Luminosity is a proxy for stellar mass, which is presumably related to the total mass of the system. Thus a relation like Tully–Fisher seems natural, with the mass of the parent halo specifying both luminosity and rotation velocity.

Luminosity is not a perfect proxy for mass. The stellar mass-to-light ratio can, and presumably does, vary with galaxy type. This leads to Tully–Fisher relations with different slopes and scatter depending on the bandpass used to measure the luminosity (e.g., Tully et al. 1998; Verheijen 2001; Courteau et al. 2007; Noordermeer & Verheijen 2007; Masters et al. 2008). Moreover, low-luminosity galaxies tend to fall below the extrapolation of the fit to bright galaxies (Persic & Salucci 1991a; Matthews et al. 1998). Yet all these observed relations presumably stem from a single underlying physical relation.

Freeman (1999) and McGaugh et al. (2000) suggested that baryonic mass is a more fundamental quantity than luminosity. For any given stellar population, different mass-to-light ratios will be produced in different bands by the same mass of stars. More importantly, physics should not distinguish between mass in stars and mass in other forms. Adding the observed gas mass to the stellar mass results in a baryonic Tully–Fisher relation (BTFR) that is linear (in log space) over many decades in mass (Verheijen 2001; Bell & de Jong 2001; Gurovich et al. 2004; McGaugh 2005b; Pfenniger & Revaz 2005; Begum et al. 2008a; Stark et al. 2009; Trachternach et al. 2009; Gurovich et al. 2010). The BTFR appears to be the fundamental physical relation underpinning the empirical Tully–Fisher relation. As such, the true form of the BTFR is of obvious importance.

In this paper, I calibrate the BTFR with gas-rich galaxies. The masses of gas-rich galaxies can be more accurately measured than those of the star-dominated galaxies that traditionally define the Tully–Fisher relation because they are less affected by the systematic uncertainty in the stellar mass-to-light ratio (McGaugh et al. 2000; Stark et al. 2009; McGaugh 2011). This results in a purely empirical calibration with a minimum of assumptions.

In Section 2, I discuss the data required to construct the BTFR, assemble samples of gas-rich galaxies, explore the statistics of the data, and calibrate the relation. In Section 3, I examine the implications of the relation for Λ cold dark matter (ΛCDM) and modified Newtonian dynamics (MOND), define a feedback efficacy parameter $\mathcal{E}$ to quantify the mapping between observations and theoretical dark halo parameters, and estimate the value of the MOND acceleration constant a_0 from the empirical BTFR. A summary of the conclusions is given in Section 4.

2. THE BARYONIC TULLY–FISHER RELATION

In order to construct the BTFR, it is necessary to estimate the baryonic mass of a galaxy on the one hand and its rotation velocity on the other. The baryonic mass is the sum of all

observed components, stars, and gas:

$$M_b = M_* + M_g. \quad (1)$$

Combining this with measurements of the rotation velocity, one obtains the BTFR:

$$M_b = AV^x. \quad (2)$$

Remarkably, this simple formula suffices to describe the data for rotating galaxies. There is no indication of any need for a third parameter such as radius or surface brightness (Zwaan et al. 1995; Sprayberry et al. 1995; Courteau & Rix 1999; McGaugh 2005a): the Tully–Fisher relation is the optimal projection of the fundamental plane of disk galaxies.

2.1. Stellar Mass

The stellar mass of a galaxy is determined from its measured luminosity and an estimate of its stellar-mass-light ratio Υ_*:

$$M_* = \Upsilon_* L. \quad (3)$$

The mass-to-light ratio is commonly obtained from stellar population models (e.g., Bell et al. 2003; Portinari et al. 2004). These predict correlations between Υ_* and color so that the observed color is used to estimate Υ_*.

The use of a stellar mass-to-light ratio estimated from stellar population models causes a significant systematic uncertainty in the stellar mass (Conroy et al. 2009), which is particularly sensitive to the initial mass function (IMF). Depending on the choice of model, one can derive BTFRs with slopes anywhere in the range of $x = 3$–4 (McGaugh 2005b). This is a basic limitation that is hard to avoid in samples of spiral galaxies where most of the baryonic mass is in the form of stars. This can be overcome by use of samples of galaxies whose baryonic mass is dominated by gas rather than stars (Stark et al. 2009). In such gas-rich galaxies, the uncertainty in stellar mass is reduced to a minor contributor to the total error budget. Nevertheless, I am careful to employ a self-consistent population model to all galaxies employed in the analysis (Table 1).

2.2. Gas Mass

Galaxies with $M_g > M_*$ can be found among very late type (Sd and Sm) spirals and irregulars with rotation velocities $V_f < 90$ km s^{-1} (e.g., Eder & Schombert 2000; Walter et al. 2008; Begum et al. 2008b; Swaters et al. 2009). With enough such galaxies, it is possible to obtain an absolute calibration of the BTFR that is effectively independent of the stellar mass estimator (Stark et al. 2009). Here I describe gas mass estimates for galaxies used in the analysis.

2.2.1. Atomic Gas

Neutral atomic (H I) gas usually dominates the gas component of disk galaxies. The mass of H I follows directly from the physics of the spin-flip transition of hydrogen, the cosmic hydrogen fraction, and the distance to each galaxy. There is no uncertain mass-to-light ratio as with stars.

The gas mass is estimated by

$$M_g = \eta M_{\rm H\,I}, \quad (4)$$

where $M_{\rm H\,I}$ is the observed atomic gas mass. The factor η accounts for the cosmic hydrogen fraction and forms of gas other than H I. Since the majority of objects of interest here are low-luminosity late-type galaxies, a primordial hydrogen fraction is assumed ($X^{-1} = 1.33$) rather than the commonly assumed solar value ($X^{-1} = 1.4$). This difference is less than the typical uncertainty in $M_{\rm H\,I}$, but does make the numbers here differ slightly from those in the source data.

2.2.2. Molecular Gas

After atomic hydrogen, molecular gas is the next significant gas component. Molecular gas persists in being difficult to detect in late-type, low surface brightness galaxies. Where detected, it appears to contain relatively little of the interstellar gas mass (Matthews & Gao 2001; O'Neil et al. 2000; O'Neil & Schinnerer

Table 1
Data for Selected Gas-rich Galaxies

Galaxy	D (Mpc)	V_f (km s^{-1})	$\log(M_*)$ ($M_\odot$)	$\log(M_g)$ ($M_\odot$)	References
DDO 210	0.94	17 ± 4	5.88 ± 0.15	6.64 ± 0.20	1,2
Cam B	3.34	20 ± 12	6.99 ± 0.15	7.33 ± 0.20	1,2
UGC 8215	4.5	20 ± 6	6.81 ± 0.15	7.45 ± 0.20	1
DDO 183	3.24	25 ± 3	7.24 ± 0.15	7.54 ± 0.20	1
UGC 8833	3.2	27 ± 4	6.94 ± 0.15	7.30 ± 0.20	1
D564-8	6.5	29 ± 5	6.76 ± 0.20	7.32 ± 0.13	3
DDO 181	3.1	30 ± 6	7.26 ± 0.15	7.56 ± 0.20	1
P51659	3.6	31 ± 4	6.67 ± 0.15	7.85 ± 0.20	1
KK98 246	7.83	35 ± 6	7.72 ± 0.15	7.93 ± 0.20	1
UGCA 92	3.01	37 ± 4	7.78 ± 0.15	8.32 ± 0.20	1
D512-2	14.1	37 ± 7	7.58 ± 0.20	7.96 ± 0.06	3
UGCA 444	0.95	38 ± 5	7.34 ± 0.15	7.75 ± 0.20	2
KK98 251	5.6	38 ± 5	7.34 ± 0.15	8.02 ± 0.20	1
UGC 7242	5.4	40 ± 4	7.57 ± 0.15	7.78 ± 0.20	1
UGC 6145	7.4	41 ± 4	7.20 ± 0.15	7.56 ± 0.20	1
NGC 3741	3.0	44 ± 3	7.24 ± 0.15	8.45 ± 0.20	1,2
D500-3	18.5	45 ± 6	6.97 ± 0.20	7.94 ± 0.05	3
D631-7	5.5	53 ± 5	6.88 ± 0.20	8.29 ± 0.15	3
DDO 168	4.3	54 ± 3	8.07 ± 0.15	8.74 ± 0.20	2
KKH 11	3.0	56 ± 5	7.28 ± 0.15	7.85 ± 0.20	1
UGC 8550	5.1	58 ± 3	8.25 ± 0.37	8.46 ± 0.39	2
D575-2	12.2	59 ± 7	7.63 ± 0.20	8.62 ± 0.07	3
UGC 4115	7.5	59 ± 6	7.77 ± 0.15	8.58 ± 0.20	1
UGC 3851	3.2	60 ± 5	8.45 ± 0.15	9.09 ± 0.20	2
UGC 9211	12.6	64 ± 5	8.12 ± 0.39	9.21 ± 0.41	2
NGC 3109	1.3	66 ± 3	7.41 ± 0.15	8.79 ± 0.20	2
UGC 8055	17.4	66 ± 7	8.09 ± 0.15	9.02 ± 0.20	1
D500-2	17.9	68 ± 7	7.41 ± 0.20	9.06 ± 0.05	3
IC 2574	4.0	68 ± 5	8.94 ± 0.15	9.20 ± 0.20	2
UGC 6818	18.6	72 ± 6	9.22 ± 0.16	9.28 ± 0.20	2
UGC 4499	13.0	74 ± 3	8.75 ± 0.27	9.32 ± 0.29	2
NGC 1560	3.45	77 ± 3	8.70 ± 0.15	9.23 ± 0.20	2
UGC 8490	4.65	78 ± 3	8.36 ± 0.15	8.96 ± 0.20	2
UGC 5721	6.5	79 ± 3	8.17 ± 0.37	9.05 ± 0.39	2
F565-V2	48.	83 ± 8	8.30 ± 0.21	9.04 ± 0.24	2
F571-V1	79.	83 ± 5	9.00 ± 0.19	9.33 ± 0.22	2
IC 2233	10.4	84 ± 5	8.96 ± 0.15	9.32 ± 0.20	2
NGC 2915	3.78	84 ± 10	7.99 ± 0.15	8.78 ± 0.20	2
NGC 5585	5.7	90 ± 3	8.98 ± 0.38	9.27 ± 0.40	2
UGC 3711	7.9	95 ± 3	8.92 ± 0.15	9.01 ± 0.17	2
UGC 6983	18.6	108 ± 3	9.53 ± 0.16	9.74 ± 0.20	2
F563-V2	61.	111 ± 5	9.41 ± 0.17	9.63 ± 0.21	2
F568-1	85.	118 ± 4	9.50 ± 0.18	9.87 ± 0.22	2
F568-3	77.	120 ± 6	9.62 ± 0.18	9.71 ± 0.22	2
F568-V1	80.	124 ± 5	9.38 ± 0.18	9.65 ± 0.22	2
NGC 2403	3.18	134 ± 3	9.61 ± 0.15	9.77 ± 0.20	2
NGC 3198	14.5	149 ± 3	10.12 ± 0.15	10.29 ± 0.20	2

References. (1) Begum et al. 2008a; (2) Stark et al. 2009; (3) Trachternach et al. 2009.

2004; Matthews et al. 2005; Das et al. 2006, 2010). Such direct measurements of molecular gas are not available for most galaxies. To estimate the molecular gas mass, we might resort to scaling relations for $M_{\rm H_2}/M_{\rm H\,I}$ such that

$$\eta = \frac{1}{X}\left(1 + \frac{M_{\rm H_2}}{M_{\rm H\,I}}\right). \quad (5)$$

Young & Knezek (1989) showed that $M_{\rm H_2}/M_{\rm H\,I}$ depends on morphological type, albeit with large scatter. From their data, McGaugh & de Blok (1997) derived the scaling relation $M_{\rm H_2}/M_{\rm H\,I} = 3.7 - 0.8T + 0.043T^2$. The vast majority of gas-rich galaxies are very late types ($T \geqslant 8$), so the typical correction is small (<5%).

We can use the recent observations of THINGS galaxies (Walter et al. 2008) to provide an independent estimate of $M_{\rm H_2}/M_{\rm H\,I}$. Leroy et al. (2008) use the observed (low) star formation in dwarf irregular galaxies to infer the amount of molecular gas present. This maps smoothly into the observed molecular content of brighter galaxies, with all disks following a relation between surface densities such that $\Sigma_{\rm H_2}/\Sigma_{\rm H\,I} = \Sigma_*/(81\ M_\odot\ {\rm pc}^{-2})$ (their Equation (33)). This is a relation between local surface densities, while a relation between global masses is desired here. The atomic gas is typically spread over a much larger area than the stars, so we cannot simply assume that the ratio of surface densities is the same as the ratio of masses. However, the respective sizes of the stellar and molecular disks are usually similar (Helfer et al. 2003). Assuming that they are the same gives

$$\frac{M_{\rm H_2}}{M_*} = \frac{\langle\Sigma_{\rm H\,I}\rangle}{81\ M_\odot\ {\rm pc}^{-2}}. \quad (6)$$

In this case, the amount of molecular mass depends on the stellar mass rather than the atomic gas mass and morphological type as in Equation (5).

In order to apply Equation (6), we need an estimate of the average H I surface density. This is almost always $<10\ M_\odot\ {\rm pc}^{-2}$ in low surface brightness galaxies (de Blok et al. 1996). In the prototypical case DDO 154, $\Sigma_{\rm H\,I} \approx 7\ M_\odot\ {\rm pc}^{-2}$ at all radii (Leroy et al. 2008). Taking this value as typical implies that molecular gas is perhaps 9% of the stellar mass of these systems. For galaxies with less than half of their mass in the form of stars, we again infer that the molecular gas makes up <5% of the baryonic mass.

For either of these estimators, the molecular gas content of H I-dominated late type galaxies is small. So small, in fact, that it is less than the uncertainty in the measurement of the H I mass in most cases. This would seem to be a good working definition of negligible, so rather than make an uncertain correction for the molecular gas mass, we neglect it entirely. In effect, we assume a constant $\eta = 1.33$.

2.2.3. Other Forms of Gas

We restrict our baryonic mass budget to the components that are actually detected, as discussed above. It is of course possible that other reservoirs of baryons exist in some undetected form. There is, however, no direct evidence for baryons in any form that is comparable in mass to the stars and atomic gas.

One conceivable reservoir of baryonic mass is hot gas in the halo. Such a component is expected in some galaxy formation scenarios. While some hot gas is certainly present, it appears that its density is too low to make a substantial contribution here (Anderson & Bregman 2010).

Another suggestion is that some of the dark matter could be in the form of undetected cold molecular gas in galaxy disks (Pfenniger et al. 1994). Pfenniger & Revaz (2005) showed that a marginal improvement in the scatter of the BTFR of McGaugh et al. (2000) could be obtained by treating η as a free parameter and suggested that the best-fit value ($\eta \approx 3$) implied additional dark baryonic mass in the disk. In more accurate data, the scatter is consistent with being caused entirely by observational uncertainties (Verheijen 2001; McGaugh 2005b; Stark et al. 2009; Trachternach et al. 2009; McGaugh 2011), nullifying this motivation for dark baryons.

In sum, there is no compelling evidence for substantial reservoirs of baryons in disk galaxies in any form other than those that are directly detected. I therefore consider only the physically motivated value of $\eta = 1.33$. Obviously, a different result would be obtained if we allowed η to include hypothetical mass components (cf. Pfenniger & Revaz 2005; Begum et al. 2008a).

2.3. Rotation Velocity

The characteristic circular velocity of a disk galaxy can be measured with resolved rotation curves or approximated by line widths. The latter is a flux-weighted integral over the velocity field and lacks the clear physical meaning of a rotation curve. It is, however, readily obtained from single disk 21 cm observations, whereas obtaining and analyzing interferometric data cubes is considerably more effort intensive (e.g., de Blok et al. 2008; Trachternach et al. 2009).

When a full rotation curve is available, one can make different choices about where to measure the circular velocity. Common choices include the maximum observed velocity ($V_{\rm max}$, e.g., Noordermeer & Verheijen 2007), which is found in the outermost measured regions where rotation curves tend toward becoming approximately flat (V_f, e.g., Verheijen 2001; McGaugh 2005b), or the velocity at some particular optical radius (e.g., Persic & Salucci 1991b; McGaugh & de Blok 1998a; Courteau & Rix 1999). The gas-rich galaxies of greatest interest here typically have gradually rising rotation curves that slowly bend over toward becoming flat without ever having an intermediate peak. For this common morphology, all these measures of velocity are very nearly equivalent. In particular, $V_{\rm max} \approx V_f$, and the velocity measured at a particular optical radius is also the same unless that radius is chosen to be very small (see Yegorova & Salucci 2007). Indeed, it is not particularly meaningful to define an optical radius for gas-rich galaxies, as the scale length of the baryonic mass can be considerably larger than that of the stars alone (McGaugh 2005a; Sellwood & McGaugh 2005).

For quantitative analysis, I restrict consideration to cases where V_f is explicitly measured, simply adopting the measured velocity from each source. For comparison purposes, I also show line-width (W_{20}) data, but do not include these data in the calibration of the BTFR as line widths, and rotation velocities are comparable but not identical measures. In order to make comparisons, I assume $V_f = W_{20}/2$ for gas-dominated galaxies with line-width measurements on the presumption that they would show rising rotation curves like those observed for comparable galaxies. For the star-dominated galaxies, I assume $W_{20}/2 = V_p = 1.1V_f$. This qualitatively accounts for the fact that bright galaxies have rotation curves that peak before falling gradually toward flatness (Persic & Salucci 1991b). The quantitative factor is chosen to reconcile the BTFR fit to $W_{20}/2$ (McGaugh et al. 2000; $A = 35\ M_\odot\ {\rm km}^{-4}\ {\rm s}^4$) with that fit to V_f

(McGaugh 2005b; $A = 50\,M_\odot$ km^{-4} s^4). This is only done to facilitate comparison between independent samples.

To account for non-circular motions, I accept whatever prescription was used by each source. In general, these corrections turn out to be rather small (cf. Tully & Fouque 1985; Oh et al. 2008; Trachternach et al. 2009; Dalcanton & Stilp 2010), as the typical velocity dispersion of low-mass galaxies is $\sim$8 km s^{-1} (Kuzio de Naray et al. 2009). Since the correction to the circular velocity occurs in quadrature, it is only somewhat important in the slowest rotators. There exist dynamically cold, rotating disks down to at least $V_f \approx 30$ km s^{-1} and perhaps as low as $\sim$10 km s^{-1} (Tikhonov & Klypin 2009).

2.4. Gas-rich Galaxy Samples

There is an enormous amount of data in the literature, but only a finite amount of it pertains to gas-dominated galaxies with $M_g > M_*$ that also have all the required information for constructing the BTFR. I describe here the accumulated data to date. I also include associated samples of star-dominated galaxies. This is done strictly for comparison as the uncertainties for star-dominated galaxies are dominated by the choice of stellar IMF. This is the systematic uncertainty that we eliminate by making use of gas-dominated galaxies. For gas-rich galaxies, the major sources of uncertainty are the 21 cm flux measurement and the distance to each galaxy. The uncertainty in the measurement of V_f is usually much smaller than that in mass (Table 1), provided that the inclination is reasonably well constrained. Cases where this condition might not be satisfied are discussed and, if suspect, excluded from fitting.

2.4.1. Stellar Mass Estimates

The data of Begum et al. (2008a), Stark et al. (2009), and Trachternach et al. (2009) constitute the sample of gas-rich galaxies for which all the necessary information is available to construct the BTFR. For these galaxies, stellar mass is, by definition, a minority of the baryonic mass. Nevertheless, we take care to estimate stellar masses self-consistently. For specificity, we use their observed $B-V$ colors and the population model of Portinari et al. (2004) with a Kroupa IMF (Kroupa 2002). Other plausible choices make no difference to the result because the gas mass dominates (Stark et al. 2009).

Several other samples are included for comparison (McGaugh et al. 2000; McGaugh 2005b; Gurovich et al. 2010). Since these data are not used in the analysis, we make no effort to reconcile them to the same population model and simply adopt the stellar mass estimated by each source. Despite the minor differences in the methods used to estimate stellar mass, these data are remarkably consistent with one another.

2.4.2. Galaxies with Rotation Curve Data

Begum et al. (2008a). Data for remarkably slowly rotating galaxies are presented and analyzed by Begum et al. (2008a, 2008b). The corrections for non-circular motions are substantial in some cases. However, the most significant difference in the analysis here is that we determine the gas mass as discussed in Section 2.2, and we select galaxies for consistency in their inclination determinations. It is not uncommon for the optical portions of gas-rich galaxies to be much smaller than their dominant H I disks (e.g., Meurer et al. 1996; Gentile et al. 2007) and for the outer H I isophotes to have a different shape than the optical isophotes (Oh et al. 2008; Trachternach et al. 2009). If the stars suffer an oval distortion (bar), then an inclination based on optical isophotes will be systematically overestimated (Mihos et al. 1997; de Blok & McGaugh 1998). Indeed, Begum et al. (2008b) observe that the optically inferred inclinations often exceed those inferred from H I. One must be wary that beam smearing might make the H I isophotes rounder than they should be, potentially causing an underestimate of inclination. To avoid either effect, I demand consistency between optical and H I inclination determinations. Specifically, I require that $\sin(i_{\rm opt})$ be within 12% of $\sin(i_{\rm H\,I})$. The restriction is placed on $\sin(i)$ because this is what matters to the accuracy with which V_f can be measured. We are concerned with the velocity at large radii, so the H I inclination is adopted (as in Begum et al. 2008a); the difference $\Delta i = |i_{\rm opt} - i_{\rm H\,I}|$ is treated as an additional source of error. The particular threshold of 12% is determined by trial and error, balancing the desire for accuracy with the need to retain at least some objects. With this criterion, 16 objects are retained from Table 1 of Begum et al. (2008a) and 12 are rejected. Requiring any greater accuracy eliminates nearly the entire sample. UGC 5456 is excluded for being marginally star dominated. Three objects are also in the sample of Stark et al. (2009).

Stark et al. (2009). Data for gas-rich galaxies are selected from the literature with an emphasis on data quality. Stark et al. (2009) required resolved rotation curves that were observed to flatten sufficiently that the logarithmic slope became <0.1 in their outer parts (see Swaters et al. 2009, from which much of this sample originates). This requirement prevents the data from skewing to low V_f due to the inclusion of galaxies whose rotation curves are still rising rapidly at the last measured point.

Trachternach et al. (2009). New WSRT observations of 11 very gas-rich galaxies selected from the sample of Schombert et al. (1997) and Eder & Schombert (2000) are used to measure both W_{20} and V_f. Of the 11 galaxies observed, six show clear evidence of rotation. Interestingly, these all have H I profiles that are double-horned or at least show some structure. Galaxies for which rotation is not positively detected tend to have single-horned profiles. Trachternach et al. (2009) discuss two methods for measuring the outer circular velocity that are largely consistent. I adopt for V_f their values measured from the position–velocity diagram ($V_{\rm pv}$ from their Table 3). For D575-2, I estimate $V_f = 59 \pm 7$ km s^{-1} based on the outermost detected 21 cm emission in their data.

McGaugh (2005b). The data for star-dominated galaxies with V_f measured from extended H I rotation curves are shown for comparison. They are not used in the analysis here. For illustration, stellar masses adopt the $\mathcal{Q} = 1$ MOND mass-to-light ratios. The BTFR fit to these data ($M_b = (50\,M_\odot$ km^{-4} s$^4)V_f^4$) can be tested by extrapolation to the much lower circular velocities of the new gas-rich galaxies.

The three data sets of Begum et al. (2008a), Stark et al. (2009), and Trachternach et al. (2009) are the most interesting for our purposes here. They compose a sample of gas-dominated galaxies with resolved rotation curve measurements. These data are listed in Table 1 and are used in the analysis. The data for these galaxies is less precise than those for bright star-dominated galaxies. However, they are more accurate, as their masses are not sensitive to systematic uncertainties in the IMF and stellar population mass-to-light ratios.

2.4.3. Galaxies with Line-width Data

Samples of galaxies with line-width data are used for comparison purposes only. We shall see that line-width data give a systematically shallower slope and greater scatter for the BTFR

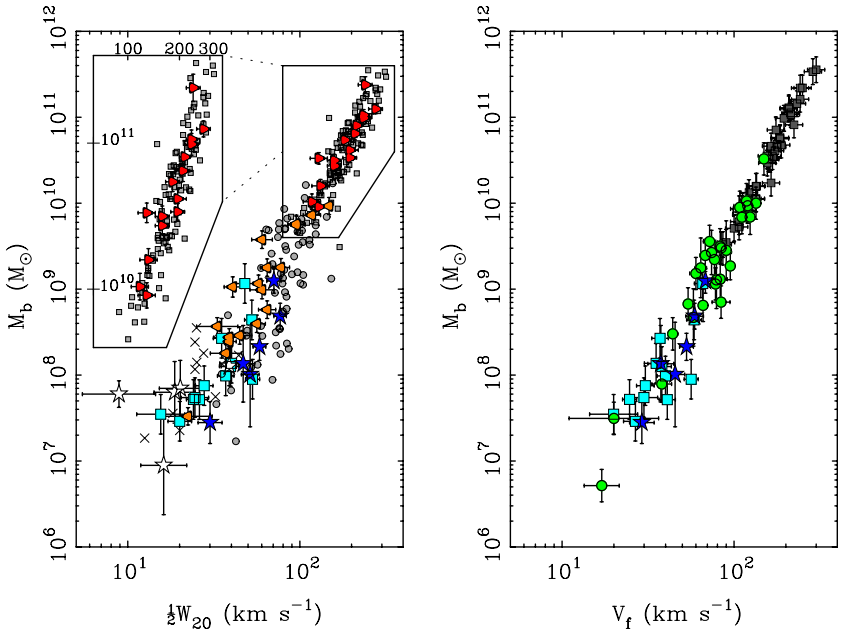

Figure 1. Baryonic mass as a function of line width (left) and circular velocity as measured from resolved rotation curves (right). Left panel: data from McGaugh et al. (2000) are shown as light gray points with uncertainties suppressed for clarity. Gas-dominated galaxies (with $M_* < M_g$) are shown as small circles and star-dominated galaxies ($M_* > M_g$) are shown as small squares. More recent data are shown with larger symbols. The data of Trachternach et al. (2009) are shown as dark blue stars in cases where rotation is detected and as open stars when it is not. The data of Begum et al. (2008a) are shown as light blue squares for cases with consistent optical and H I inclinations and as crosses in cases where these differ substantially. The H I data of Gurovich et al. (2010) are shown as orange left-pointing triangles. The data of the star-dominated galaxies of Sakai et al. (2000) are shown as red right-pointing triangles with stellar mass from the *H*-band data of Gurovich et al. (2010). The two samples of star-dominated galaxies are compared in the inset. This also serves to illustrate the range covered by the bright spirals that traditionally define the Tully–Fisher relation—a range that is vastly expanded by the inclusion of gas-rich dwarfs. In the right panel, data for galaxies with V_f measured from resolved rotation curves include the rotating cases of Trachternach et al. (2009), the data of Begum et al. (2008a) with consistent inclinations, the gas-dominated galaxies compiled by Stark et al. (2009, green circles), and the star-dominated galaxies compiled by McGaugh (2005b, dark gray squares).

(A color version of this figure is available in the online journal.)

than do rotation curve data. This appears to be a limitation of the line width as a proxy for the rotation velocity. Aside from this detail, the data present a consistent overall picture.

McGaugh et al. (2000). Gas-rich galaxies were selected from the sample of Schombert et al. (1997) and Eder & Schombert (2000) to have inclinations $i > 45°$. Stellar masses were estimated from *I*-band data assuming a constant mass-to-light ratio ($\Upsilon^I_* = 1.7\ M_\odot/L_\odot$). We retain this original prescription, making only the correction to stellar mass discussed by Gurovich et al. (2004). Data for star-dominated galaxies with *H*-band photometry were taken from Bothun et al. (1985). A constant *H*-band mass-to-light ratio of $\Upsilon^H_* = 1\ M_\odot/L_\odot$ was assumed. These data are included here for comparison to more recent data but are not used in the analysis.

Gurovich et al. (2010). New data are presented for galaxies with $M_g > M_*$. Detailed stellar population modeling has been performed to determine the stellar mass (Table 11 of Gurovich et al. 2010). The same modeling procedure has also been applied to the star-dominated sample of Sakai et al. (2000). We adopt the stellar mass determinations based on *H*-band photometry[1] for these galaxies (Table 4 of Gurovich et al. 2010) to facilitate direct comparison with the data of Bothun et al. (1985) employed by McGaugh et al. (2000). All of the bright galaxies of Sakai et al. (2000) have nicely double-horned line profiles with well-measured line widths. This is not the case for the new gas-rich galaxies presented by Gurovich et al. (2010), for which the H I profiles are all narrow and single-horned (S. Gurovich 2010, private communication). Such profiles can be poor indicators of V_f (Trachternach et al. 2009).

2.5. Comparison of the Data

Figure 1 shows the data. Over all, the agreement between the various data is good. This is true even for the star-dominated galaxies, despite the differences in the population modeling. The spiral galaxies of Sakai et al. (2000) fall in the midst of the data of Bothun et al. (1985, inset of Figure 1) with indistinguishable slope and normalization. The chief difference is the lower scatter in the data of Sakai et al. (2000). This presumably results from the more accurate distances to the individual galaxies based on *Hubble Space Telescope* (*HST*) observations (Freedman et al. 2001). This is expected: As the data improve, the scatter is reduced. Indeed, essentially all of the scatter can be accounted for by observational uncertainty and the expected variation in stellar mass-to-light ratios (Verheijen 2001; McGaugh 2005b; Stark et al. 2009).

The scatter is larger for lower luminosity galaxies. This is also expected: It is more challenging observationally to obtain precise data for faint dwarfs than it is for bright spirals. Nevertheless, the data for the gas-rich dwarfs appear to be largely consistent. Moreover, the scatter is reduced as we progress from line widths to resolved measures of the rotation velocity (left versus right panels in Figure 1). The improved accuracy with which the rotation velocity is measured is reflected in reduced scatter.

There are some outliers among the gas-rich dwarfs, especially when W_{20} is used as the velocity estimator. The two most

[1] Whether optical or *H*-band data are used to estimate the stellar mass for the bright galaxies of Sakai et al. (2000) makes a difference to the slope of the BTFR: $x = 3$ in the optical and $x = 4$ in the *H* band. This exemplifies the systematic uncertainty that gas-dominated galaxies save us from.

dramatic outliers from the sample of Begum et al. (2008a) are UGC 3755 and KK98-65, which fall far to the left of the main correlation. These are rejected by the requirement of consistent optical and H I inclinations, as are a number of galaxies that do lie along the BTFR in Figure 1 when the H I inclination is used. The outliers from Trachternach et al. (2009) are those objects for which rotation is not clearly detected (D575-5 is the most discrepant case). Three objects from the sample of Gurovich et al. (2010) stand out from the rest of the data: ESO 085-G 088, AM 0433-654, and HIPASS J1424-16b. ESO 085-G 088 has a large velocity error, so its status as an outlier is only marginal. The other two objects clearly deviate from the rest of the data, including the bulk of the data of Gurovich et al. (2010). Since we do not have resolved measures of rotation for these objects, it is possible that they, like the single-peaked H I profiles of Trachternach et al. (2009), would not show clear evidence of rotation if so observed. Another possibility is that the optical inclinations used by Gurovich et al. (2010) are systematically in error as discussed in Section 2.4.2. Lacking resolved H I observations, we cannot make the same consistency check that is possible with the data of Begum et al. (2008a). The inclination of AM 0433-654 is 43° and that of HIPASS J1424-16b is 47°. A shift of ∼0.15 dex in W_{20} would reconcile these galaxies with the other data. If inclination is responsible, the corresponding inclinations would be 29° for AM 0433-654 and 31° for HIPASS J1424-16b. From experience with such objects (e.g., de Blok & McGaugh 1998; Trachternach et al. 2009), this is well within the realm of possibility. Indeed, it would be surprising if something like this did not happen with only optical inclinations to work with.

Over all, the data paint a consistent picture (Figure 1) despite the inevitable concern over the accuracy of a few individual measurements. The BTFR is continuous and linear in log space over five decades in mass. There is a hint of curvature when W_{20} is used as the rotation velocity measure, but it is not statistically significant. There is not even a hint of curvature when resolved rotation curves are available to measure V_f.

We expect the accuracy of the data to improve as we move from integral measures like the line width to physically meaningful rotation velocities measured from resolved H I data cubes. This expectation is realized in the reduced scatter seen in the right panel of Figure 1. We can quantify this with ordinary least-squares fits to the data.

If we apply the maximum likelihood method of Weiner et al. (2006) to fit the new line-width data (i.e., all the data in the left panel of Figure 1 except those of McGaugh et al. 2000), we obtain a slope $x = 3.41 \pm 0.08$ and an intercept $\log A = 2.91 \pm 0.17$. If we perform the same exercise with the rotation curve data in the right panel of Figure 1, we obtain $x = 3.94 \pm 0.11$ and $\log A = 1.81 \pm 0.22$. These formal fits have rather different slopes even though the chief difference is in the scatter. The method of Weiner et al. (2006) accounts for uncertainties in both velocity and mass, and can optionally estimate the amount of intrinsic scatter in a sample. Accounting for the stated observational errors (e.g., Weiner et al. 2006) implies an intrinsic scatter in the line-width data of ∼0.2 dex. That is, there is 0.2 dex of scatter not explained by observational uncertainty. In contrast, this number is zero for the rotation curve data in the right-hand panel: Observational errors suffice to explain all the scatter, leaving no room for intrinsic scatter. This difference in scatter implies some source of variance in line-width measures that is perhaps not accounted for in the stated uncertainties, and not likely to be meaningful to the physics we are interested in here.

At least part of the reason for the difference in fitted slopes is physical: W_{20} is not a perfect proxy for V_f. Bright galaxies typically have peaked rotation curves with $V_{\rm max} > V_f$. Line-width measurements do not resolve where emission originates and are thus sensitive to the maximum velocity rather than that at larger radius. This immediately skews the slope to shallower values. A similar if less pronounced effect can be seen in optical rotation curves that are resolved but not particularly extended (Torres-Flores et al. 2011).

For the physical interpretation of the BTFR, we wish to have as precise a probe as possible of the quantity of interest. For ΛCDM, this would be the virial velocity of the dark matter halo. In the case of MOND, we need a measure that probes the low acceleration regime. In both cases, V_f provides a better measure than W_{20}.

2.6. Statistics of the Gas-rich Galaxy Data

2.6.1. Slope

The slope of the BTFR has been addressed by many authors (e.g., McGaugh et al. 2000; Bell & de Jong 2001; Gurovich et al. 2004, 2010; McGaugh 2005b; Begum et al. 2008a; Stark et al. 2009) and is typically found to be between $x = 3$ and 4. Most of this variation is due to the prescription adopted for estimating the mass-to-light ratio (McGaugh 2005b), which is by far the strongest systematic effect. This can be remedied by selecting gas-dominated galaxies as described in Section 2.4.1.

Stark et al. (2009) found a slope $x = 3.94 \pm 0.07$ with a bisector fit while Gurovich et al. (2010) found $x = 3.0 \pm 0.2$ from their gas-dominated galaxies (their Table 12). These results appear to be contradictory. Repeating the analysis of Gurovich et al. (2010), I obtain the same result. However, simply looking at the data, it is not obvious that they are in conflict. Part of the difference is simply the difference in velocity estimators, as line widths give shallower slopes than resolved rotation velocities. Their sample is also small, so is easily influenced by a few outliers as discussed above (Section 2.5).

This difference between $x \approx 3$ and 4 is precisely the difference between the nominally anticipated slopes in ΛCDM and MOND. The correct answer is therefore of considerable importance and lends itself to controversy. Bear in mind that the data themselves are quite consistent (Figure 1), so any controversy is in the fitting and choice of velocity estimator, not in the data. The line width is a convenient proxy for the rotation velocity when resolved rotation curves are unavailable, but not a substitute for them when predictive theories are being tested.

To illustrate the difference between slopes of 3 and 4, we rotate the BTFR into a new coordinate system (ℓ,δ) parallel to it such that ℓ measures the position of a galaxy along the BTFR and δ its deviation perpendicular to it. That is,

$$\ell = \cos\theta \log V_f + \sin\theta(\log M_b - \log A) \quad (7)$$

$$\delta = \cos\theta(\log M_b - \log A) - \sin\theta \log V_f, \quad (8)$$

where $\tan\theta$ is the slope of the BTFR. In Figure 2, we show the data rotated into the frames defined by the fits of Gurovich et al. (2010) with slope $\tan\theta = 3$ and McGaugh (2005b) with $\tan\theta = 4$.

A slope of 4 does a good job of describing the bulk of the data: There is no systematic deviation from the dotted line in the lower panel of Figure 2. In contrast, there is an obvious

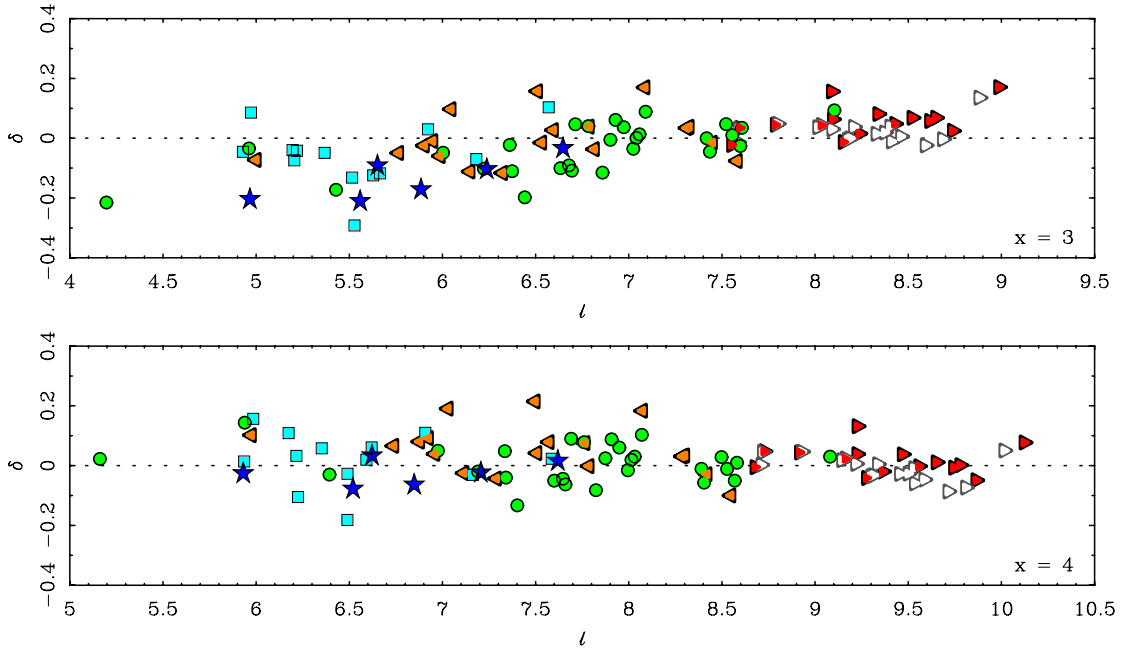

Figure 2. Data in a coordinate system rotated (Equations (7) and (8)) so that the abscissa is the position of a galaxy along the BTFR and the ordinate is its perpendicular distance from the BTFR. Symbols as per Figure 1 with the exception that the star-dominated galaxies of Sakai et al. (2000) are shown twice: once with the *H*-band stellar masses of Gurovich et al. (2010) as in Figure 1 and again for the hybrid *V*- and *H*-band stellar masses of Gurovich et al. (2010, open right-pointing triangles). This illustrates the systematic uncertainty that plagues star-dominated galaxies but from which gas-dominated galaxies are largely immune. The top panel shows the BTFR with slope 3 fit to the data of Gurovich et al. (2010). The bottom panel shows the BTFR fit of McGaugh (2005b) with slope 4. The data shown in the bottom panel are independent of those to which the fit was made.

(A color version of this figure is available in the online journal.)

residual from a slope of 3 in the top panel. The data show a clear preference for the steeper slope.

Figure 2 also illustrates the systematic caused by different mass-to-light ratio estimates for star-dominated galaxies. The galaxies from Sakai et al. (2000) are shown twice, once with masses based on *H*-band data (Table 4 of Gurovich et al. 2010) and again with the average of *V*- and *H*-band stellar masses (Table 5 of Gurovich et al. 2010). The hybrid *V*–*H* masses are nicely consistent with a slope of 3, while *H* alone prefers a slope of 4. While one must choose which band to trust for bright galaxies, this choice is rendered irrelevant for gas-dominated galaxies. We therefore concentrate the rest of our analysis on the gas-rich galaxy sample described in Sections 2.4.2 and 2.4.1.

Taking the 47 gas-rich galaxies with reasonably trustworthy data (Table 1), the best-fit slope is $x = 3.82 \pm 0.22$ with intercept $\log A = 2.01 \pm 0.41$. Various methods (forward, reverse, and maximum likelihood) all give the same result. Of these data, the velocity measurements of Begum et al. (2008a) are the most challenging: Only three of their objects meet the quality criteria of Stark et al. (2009). Excluding the data of Begum et al. (2008a) but retaining those of Stark et al. (2009) and Trachternach et al. (2009) gives $x = 4.05 \pm 0.29$ from a forward fit, 3.92 ± 0.29 from a reverse fit, and a bisector slope (Isobe et al. 1990) of 3.98 ± 0.06. The corresponding intercepts are $\log A = 1.57$, 1.82, and 1.71, respectively, with uncertainty ± 0.24. The slight difference that occurs when also fitting the data of Begum et al. (2008a) may result from a slight skew to low velocities and testifies to the difficulty in obtaining quality data for very slow rotators (see also Trachternach et al. 2009). The skew effect becomes more pronounced if we relax the selection criterion that requires consistent optical and H I inclination determinations. Irrespective of these details, these fits are all consistent with one another (Figure 3), and none yield a slope that is meaningfully different from 4.

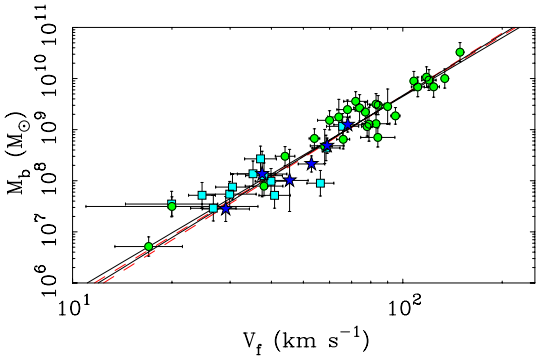

Figure 3. Fits to the BTFR of gas-dominated galaxies. Symbols as per Figure 1. The solid lines show the best fit to the whole sample (with slope $x = 3.82$) and the bisector (slope 3.98) of the forward and reverse fits (dashed lines) limited to the samples of Stark et al. (2009) and Trachternach et al. (2009)—that is, excluding the less accurate points (squares) from Begum et al. (2008a). The various fits are consistent within the uncertainties and yield the same basic result.

(A color version of this figure is available in the online journal.)

2.6.2. Normalization

An interesting question we can pose to the gas-rich galaxy data is what the normalization of the BTFR is with slope fixed to 4. The gas-rich galaxies provide an absolute calibration of the BTFR that is very nearly independent of the estimator we use for the stellar mass-to-light ratio. By fixing the slope, we can sharpen our estimate of the intercept and also examine higher order moments of the distribution. In addition to the scatter perpendicular to the BTFR, σ_δ, we can also examine the skew α_3 and kurtosis $\hat{\alpha}_4$.

Table 2 shows these statistics for several combinations of the rotation curve samples. We start with the sample of Stark et al. (2009) as their sample was constructed for this exercise.

Table 2
Statistics of Gas-rich Galaxy Rotation Curve Samples

Sample	N	χ^2_ν	log A Weighted	log A Unweighted	α_3 Skew	$\hat{\alpha}_4$ Kurtosis	a_0 Weighted	a_0 Unweighted
S	28	1.04	1.71	1.65	−0.07	−0.14	1.18	1.36
ST	34	0.92	1.67	1.64	−0.01	0.01	1.30	1.39
STB	47	0.99	1.69	1.71	−0.13	−0.10	1.24	1.18

Notes. Samples: S: Stark et al. (2009); T: Trachternach et al. (2009); B: Begum et al. (2008a). The units of A are $M_\odot$ km^{-4} s^4 and those of a_0 are Å s^{-2}. The skew and kurtosis are the statistics of the orthogonal deviations δ (Equation (8)).

Adding the galaxies of Trachternach et al. (2009) decreases the intercept slightly. Adding the data of Begum et al. (2008a) raises again, back near to the value found by McGaugh (2005b, log $A = 1.70$).

Table 2 gives quantitative estimates for the intercept. For each combination of samples both a weighted and an unweighted estimate is given. The weighted estimate comes from minimizing χ^2_ν by adjusting log A with fixed slope: we minimize the orthogonal deviations. The unweighted estimate is made by finding the centroid of the distribution in the orthogonal deviations δ of the rotated data and requiring the centroid to lie at $\delta = 0$. The latter method gives no heed to the accuracy of the data, but is less sensitive to the influence of outliers whose formal uncertainty may understate systematic effects. These methods give indistinguishable results.

All combinations of the various samples give consistent estimates for the intercept. To be specific, we adopt the weighted estimate from the combination of the Stark–Trachternach sample:

$$A = 47 \pm 6\, M_\odot \text{ km}^{-4} \text{ s}^4. \quad (9)$$

This is the midpoint of the various determinations and has the smallest χ^2. This value is of course very similar to the unweighted value (45 $M_\odot$ km^{-4} s^4) obtained from the Stark et al. (2009) sample alone (McGaugh et al. 2010; McGaugh & Wolf 2010). It is also similar to the value (50 $M_\odot$ km^{-4} s^4) found by McGaugh (2005b) from star-dominated galaxies, but has the virtue of being completely empirical with little sensitivity to how stellar masses are estimated.

It appears that at this juncture, systematic effects and the necessary assumptions are as limiting as data quality. It is traditional to assume $\eta = 1.4$, which is appropriate for solar metallicity atomic gas, but is slightly larger than the primordial 1.33 taken here for these little evolved, gas-rich, low-mass galaxies. The choice of $\eta = 1.4$ is not important to the star-dominated galaxies in McGaugh (2005b), but we note that adopting it here would cause a change in mass of at most 5% (for purely gaseous galaxies) that would drive $A = 47 \rightarrow 49\, M_\odot$ km^{-4} s^4. This is at the level of our best guess in the mass of molecular mass. At this level the systematic uncertainty in the IMF that plagues stellar mass estimates also begins to play a role even in gas-dominated galaxies. Given these considerations, any value in the range 45–50 $M_\odot$ km^{-4} s^4 is plausible, with values far outside this range quickly becoming less plausible. If we use the BTFR to estimate stellar masses (Stark et al. 2009), then more massive star-dominated galaxies are consistent with a Kroupa IMF. Grossly different stellar masses would imply a break in the slope of the relation around ∼100 km s^{-1} where the galaxy population transitions from frequent to infrequent gas domination.

2.6.3. Scatter

The scatter in our rotated coordinates is $\sigma_\delta = 0.06$ with only the third digit varying from sample to sample. In terms of mass this is 0.24 dex. The bulk of this uncertainty (0.20 dex) is provided by the error in the baryonic mass. Velocity uncertainties are less important in most samples, and only rival the uncertainty in mass in the lowest mass systems. Together, the uncertainties in mass and rotation velocity suffice to account for essentially all of the observed scatter.

A robust estimator of the dispersion of a sample is the median absolute deviation (MAD). The dispersion of the various samples about the BTFR as measured by their MAD is shown in Figure 4. Also shown is the median measurement uncertainty $\langle\sigma\rangle$. For data that scatter about the relation simply because of observational uncertainty, $\langle\sigma\rangle \rightarrow 1.48$MAD as N becomes large presuming there are no systematic uncertainties that have not been accounted for. Figure 4 shows that indeed $\langle\sigma\rangle \approx 1.48$MAD in most cases. This leaves little, if any, room for intrinsic scatter in the BTFR. Indeed, the only times when scatter measured by the MAD significantly exceeds that expected from measurement errors are in the cases where we have identified systematic uncertainties that are not included in the error estimate: In the subset of the sample of Trachternach et al. (2009) where no signature of rotation has been detected, and in the sample of Begum et al. (2008a) where the optical and H I inclination estimates differ greatly. Had we been unaware of these sources of systematic error, we might infer some finite intrinsic scatter. Instead, it appears that including less accurate data merely increases the scatter as one would expect.

The BTFR of gas-rich galaxies appears to have essentially zero intrinsic scatter. The same conclusion follows from noting that χ^2_ν is close to unity (Table 2). A finite intrinsic width to the relation would cause $\chi^2_\nu > 1$ (Weiner et al. 2006). We can place an upper limit on the scatter by assuming that the data are Gaussian (a dubious but conservative assumption for this purpose) and subtracting the measurement error in quadrature from 1.48MAD. This gives a limit on the intrinsic scatter of $\sigma_{\rm int} < 0.15$ dex in mass for the Stark et al. (2009) sample and $\sigma_{\rm int} < 0.18$ for the trimmed sample of Begum et al. (2008a). Essentially zero intrinsic scatter is inferred by this method for the gas-rich data of Gurovich et al. (2010) or the star-dominated galaxies of Sakai et al. (2000). For the data of Trachternach et al. (2009), the expected error exceeds the observed scatter. This might indicate that the uncertainties (especially in distance) have been overestimated, but the sample is small so we should not expect the assumption of a normal distribution to hold. Indeed, that is generally true here, which mitigates against there being much intrinsic scatter.

It is common in extragalactic astronomy for correlations between physical quantities to exhibit lots of scatter. In the BTFR we seem to have a relation with little or no intrinsic scatter. There are some possible couple of caveats to this. First, it is conceivable that the uncertainties in the data have been overestimated. Second, selection effects might limit the sample to only those objects that obey the BTFR.

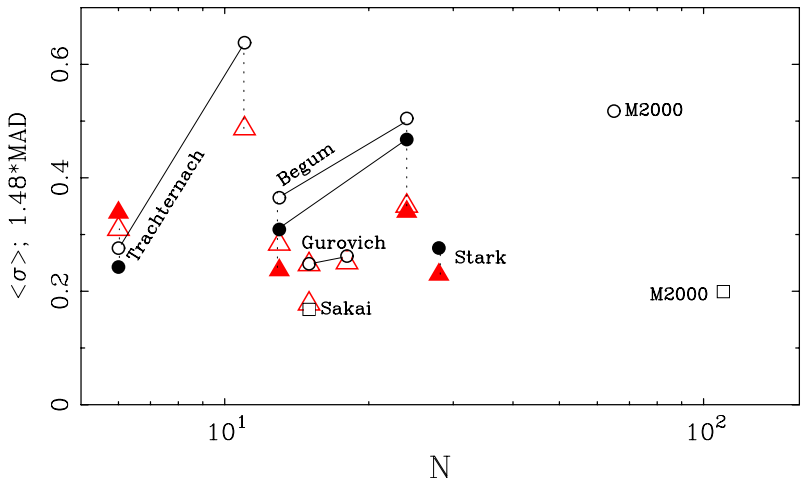

Figure 4. Median error (triangles) and median absolute deviations (MADs) of the various samples. Open symbols refer to line-width measurements; solid symbols represent rotation curve measures. Lines connect samples that have been trimmed for quality as discussed in the text, showing both trimmed and untrimmed samples. Samples are labeled by first author with the MAD of gas-dominated galaxies represented by circles and that of star-dominated galaxies by squares. The MAD is a robust estimator of the dispersion of a sample; for a normal distribution $\sigma = 1.48$MAD. The similarity of the observed scatter to the typical uncertainty is an indication that the BTFR has very little intrinsic scatter.

(A color version of this figure is available in the online journal.)

Overestimation of the uncertainties seems unlikely. That $\chi^2_\nu \approx 1$ is a sign not only that the model is a reasonable description of the data, but also that the uncertainties have been neither over nor underestimated. Even if the data were arbitrarily accurate, so that all of the observed scatter is intrinsic, the intrinsic width of the relation is still small: the observed 0.24 dex. If anything, this would appear to confirm that the disks of the selected galaxies are well-behaved dynamically cold rotators. If it were otherwise, e.g., if there were substantial non-circular motions in the disks of these galaxies, then this would be a substantial source of intrinsic scatter and the observed scatter would be much larger (Franx & de Zeeuw 1992; Trachternach et al. 2009).

It is more difficult to address the issue of potential selection effects. However, in the time since Zwaan et al. (1995), the persistent surprise has been how tight the Tully–Fisher relation remains when challenged with data for new types of galaxies that we would naively expect to deviate from it. Since this exercise has now been performed by many different observers for many different types of galaxies, it seems unlikely that selection effects play a significant role in suppressing the scatter of the BTFR. We select gas-rich galaxies here, but it is already well established that star-dominated galaxies obey the BTFR with little scatter (e.g., Verheijen 2001; McGaugh 2005b; Noordermeer & Verheijen 2007). The only further selection made here is on data quality. When lower quality data are admitted, the scatter increases (Figures 1 and 4), just as one would expect. There is no clear evidence for intrinsic scatter beyond that induced by observational uncertainty and the systematic effects inevitable in astronomical data.

It is impossible to estimate the scatter that might result from including objects that are not already included. We have restricted our discussion to rotating galaxies, since these are the objects that define the Tully–Fisher relation. It is not obvious that it should apply to non-rotating galaxies, though the Faber–Jackson relation for elliptical galaxies provides an obvious analog. Dwarf spheroidal galaxies fall remarkably close to the BTFR with a simple estimate of the equivalent rotation velocity ($V_f = \sqrt{3}\sigma$; Wolf et al. 2010) though the ultrafaint dwarfs fall systematically below it (McGaugh & Wolf 2010). Even objects that have no apparent business adhering to the BTFR either do so or come surprisingly close to doing so (e.g., the H I ring in Leo). Among rotating disk galaxies, one would expect differences in the baryonic mass distribution to have some impact on the BTFR, just because $V_f^2 \propto GM/R$. And yet disk-dominated spirals, bulge-dominated early-types, diffuse low surface brightness galaxies, and dwarf irregulars all adhere to the same BTFR in spite of their palpably different mass distributions (Zwaan et al. 1995; Sprayberry et al. 1995; Tully & Verheijen 1997; McGaugh & de Blok 1998a; Courteau & Rix 1999; Verheijen 2001; Noordermeer & Verheijen 2007). Rather than finding greater scatter as we expand our samples beyond the Sc I galaxies traditionally utilized in distance scale studies, we find that rotating galaxies of all types adhere to the same BTFR. It therefore seems unlikely that there remains some large, unknown population of galaxies in rotational equilibrium that would induce substantial scatter in it.

2.6.4. Skew and Kurtosis

A persistent problem with interpreting astronomical data is whether Gaussian statistics actually apply. One reason for this is that systematic errors often dominate random ones. We can check whether this might be an issue here by examining higher order statistics like the skew (lopsidedness) and kurtosis (pointiness) of the distribution in the deviations δ perpendicular to the BTFR. If the data are well behaved (i.e., distributed normally), the skew and kurtosis should be small.

For all three combinations of samples in Table 2, both the skew and the kurtosis are small: $|\alpha_3|$ and $|\hat{\alpha}_4| < 0.15$. These samples are consistent with normal distributions as they should be if random errors dominate over systematic effects. This is especially true for the combination of the Stark et al. (2009) and Trachternach et al. (2009) samples, which have $|\alpha_3| = \hat{\alpha}_4 = 0.01$.

For comparison, the sample of Gurovich et al. (2010) has $\alpha_3 = 0.63$ and $\hat{\alpha}_4 = -0.51$ around their best fit. If we trim the three outlying galaxies discussed in Section 2.5, the skew is reduced ($\alpha_3 = -0.15$) but the kurtosis grows ($\hat{\alpha}_4 = -1.28$). The negative kurtosis means that the distribution is flat topped: It does not have a well-defined central peak as it should

if the data simply scatter around the correct relation. These data are not distributed normally. This undermines the basic assumption of the least-squares fitting method, so the apparently straightforward fit of Gurovich et al. (2010) yields a misleading constraint on the slope.

3. DISCUSSION

Understanding the physical basis of the BTFR is central to one of the most fundamental issues presently confronting extragalactic astronomy. The BTFR provides a simple test that in principle can distinguish between ΛCDM and MOND (Milgrom 1983). Here we discuss the interpretation of the BTRF in terms of each paradigm in turn.

3.1. ΛCDM

The interpretation of the BTFR in ΛCDM depends on how we relate dark and baryonic mass. Different assumptions can plausibly be made, leading to rather different interpretations. Here we start from general considerations, later proceeding to specific models.

It is conventional in cosmology to refer to structures by the density contrast they represent with respect to the critical density of the universe. The mass enclosed within a radius encompassing the overdensity Δ is

$$M_\Delta = \frac{4\pi\Delta}{3}\rho_{\rm crit} R_\Delta^3. \quad (10)$$

With $\rho_{\rm crit} = 3H_0^2/8\pi G$, this becomes

$$M_\Delta = \frac{\Delta}{2G} H_0^2 R_\Delta^3. \quad (11)$$

By the same token, the circular velocity of a tracer particle at R_Δ is $V_\Delta^2 = GM_\Delta/R_\Delta$. Consequently,

$$M_\Delta = (\Delta/2)^{-1/2}(GH_0)^{-1}\ V_\Delta^3. \quad (12)$$

In ΛCDM, the density contrast $\Delta \approx 100$ marks the virial extent of a dark matter halo (Eke et al. 2001). For $H_0 = 72\ {\rm km\,s^{-1}\,Mpc^{-1}}$,

$$M_{\rm vir} = (4.6 \times 10^5\ M_\odot\ {\rm km^{-3}\ s^3}) V_{\rm vir}^3. \quad (13)$$

This includes all mass, dark and baryonic, that reside within the radius $R_{\rm vir}$.

Dark matter halos thus obey a scaling relation reminiscent of the Tully–Fisher relation (e.g., Steinmetz & Navarro 1999). This is not the same as the observed Tully–Fisher relation, as both mass and velocity refer to a radius $R_{\rm vir}$ that is much larger than what is observed. In order to map these theoretical quantities into the observed baryonic mass M_b and circular velocity V_f, we need to introduce some factors:

$$M_b = f_d f_b M_{\rm vir} \quad (14)$$

and

$$V_f = f_V V_{\rm vir}. \quad (15)$$

The total mass of baryons available within $R_{\rm vir}$ is $f_b M_{\rm vir}$, where f_b is the cosmic baryon fraction ($f_b = 0.17$; Komatsu et al. 2009). The factor f_d represents the fraction of these available baryons that contribute to the observed baryonic mass. Similarly, the observed velocity need not be identical to $V_{\rm vir}$; hence the factor f_V.

3.1.1. General Constraints

The BTFR would follow from Equation (13) with a slope of $x = 3$ and a normalization $\log A = 4.74$ if $f_d = f_V = 1$. This is shown as the dashed line in Figure 5. Had this matched the data, it would provide a very satisfactory interpretation (Steinmetz & Navarro 1999). Instead, it exceeds the data, leading us to consider models with $f_d < 1$ and $f_V \neq 1$.

Equations (13)–(15) provide a generic constraint on ΛCDM galaxy formation models. These typically invoke feedback to suppress the cold baryon content of disks so that $f_d < 1$. We define a feedback efficacy parameter

$$\log \mathcal{E} \equiv 3 \log f_V - \log f_d. \quad (16)$$

When $f_V = 1$, $\mathcal{E}$ is just the inverse of f_d, so a galaxy with $\mathcal{E} = 10$ has lost 90% of its baryons, and one with $\mathcal{E} = 100$ has lost 99% of them. By "lost" we mean that they are not part of the disk of stars and cold gas that contribute to M_b in the BTFR. It is irrelevant whether these baryons have been physically expelled as envisioned in many feedback models or remain in the halo in some dark, unobserved form. $\mathcal{E}$ merely tells us how effective feedback (or any other mechanism) has been in suppressing the inclusion of the available baryons into the observed disk.

In addition to variations in f_d, the mapping of the observed to virial velocity f_V can also play a role. This ratio can easily vary with mass as more massive disks boost f_V by engendering more adiabatic contraction in their host dark matter halos than low-mass disks (e.g., Bullock et al. 2001). My own experience with modeling adiabatic contraction (Sellwood & McGaugh 2005) leads me to expect this to be a modest effect, most likely in the range $1 \leqslant f_V \leqslant 1.3$. Very recently, Reyes et al. (2011) have combined dynamical and gravitational lensing measurements to estimate $f_V \approx 1.3$ for galaxies with $M_* > 6 \times 10^9\ M_\odot$. This represents the upper end of the BTFR (roughly $V_f > 100\ {\rm km\,s^{-1}}$). In order to help with the observed variation in $\mathcal{E}$, f_V would need to be substantially less in lower mass galaxies. While these often have rising rotation curves (so, possibly $f_V < 1$), flatness of the rotation curve is an explicit selection criterion of the Stark et al. (2009) sample. For these galaxies, $f_V \approx 1$ seems the best guess, as their disks are not massive enough to substantially alter their dark matter halos to yield $f_V > 1$, nor does it seem likely that the rotation curve will resume rising after being observed to flatten out so as to yield $f_V < 1$. For the very low mass galaxies of Begum et al. (2008a), $f_V < 1$ is certainly possible, but it seems unlikely to be tiny. If $f_V = 0.9$ at $V_f = 30\ {\rm km\,s^{-1}}$ and 1.3 at $300\ {\rm km\,s^{-1}}$, the total variation in $\mathcal{E}$ is a factor of three. This does not, by itself, suffice to explain the data.

Equation (16) maps between the parameters of the dark matter halo and those of the disk galaxy it hosts. It is completely general, encompassing what needs to happen to connect theory with observational reality. In order to be consistent with the data presented here, models must meet the requirement

$$\log \mathcal{E} = 1.2 - \log\left(\frac{V_f}{100\ {\rm km\,s^{-1}}}\right) - \frac{1}{2}\log\left(\frac{\Delta}{100}\right). \quad (17)$$

This constraint applies to models of disk galaxies over the range $30\ {\rm km\,s^{-1}} < V_f < 300\ {\rm km\,s^{-1}}$. In applying this constraint, care should be taken to use consistent definitions of total mass (M_Δ with $\Delta = 100$) and rotation velocity. The term involving Δ is a simple shift in normalization that translates to other common definitions of halo mass (e.g., $\Delta = 200$ instead of 100). The

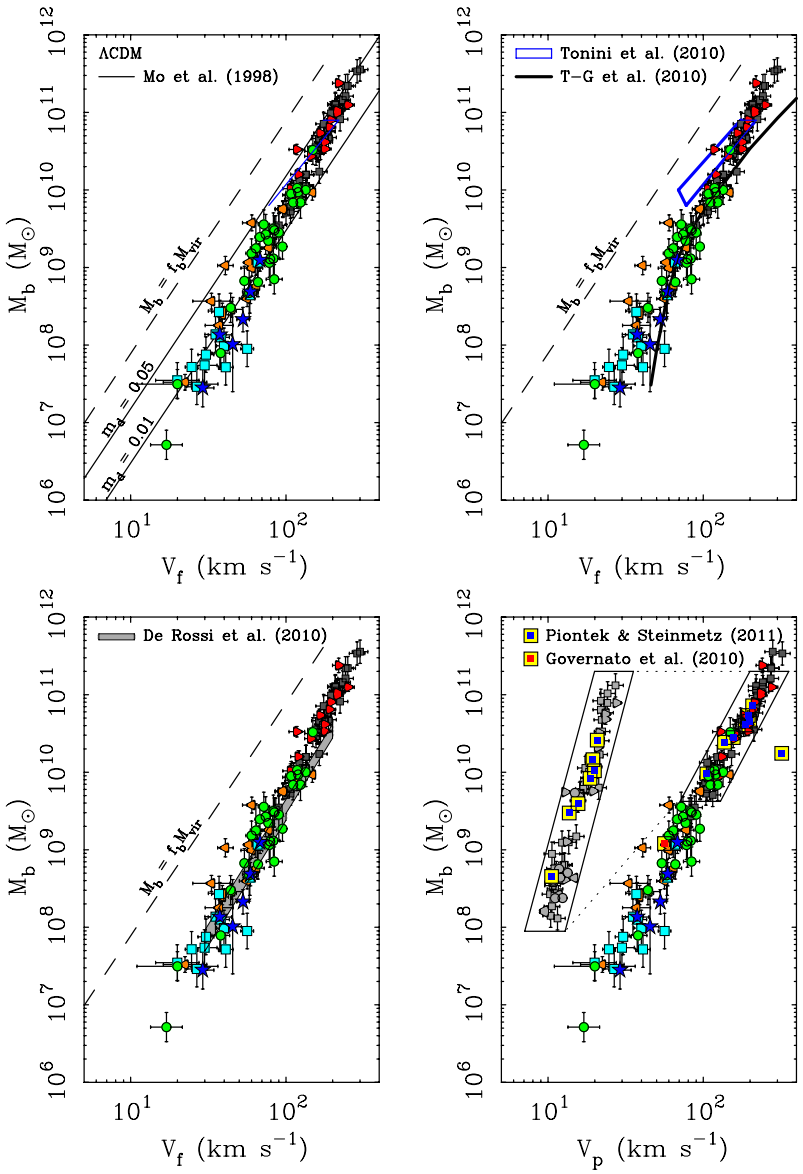

Figure 5. BTFR in ΛCDM. Symbols as per Figure 1. The dashed line illustrates the baryons that are available within the virial radii of dark matter halos with $V_{\rm vir} = V_f$. Solid lines in the top left panel illustrate the model of Mo et al. (1998) for two choices of their disk fraction parameter m_d. In the top right panel, the curved solid line is the model of Trujillo-Gomez et al. (2011), while the box illustrates the range of the model of Tonini et al. (2010). The bottom left panel shows the model of de Rossi et al. (2010). The bottom right panel plots the model galaxies of Piontek & Steinmetz (2011) and Governato et al. (2010) along with the data. Here the peak rotation velocity V_p is used, as this is more directly comparable to the models of Piontek & Steinmetz (2011). The inset shows that these agree quite well with the data for star-dominated galaxies.

(A color version of this figure is available in the online journal.)

constraint holds irrespective of the particular choice of definition for halo mass.

Equation (17) is a scaling between $\mathcal{E}$ and rotation velocity. That the efficacy of feedback scales with velocity is not surprising, as the shallower potential wells of low-mass halos should be less effective at retaining baryons. The efficacy of feedback should also depend on the physics driving it. For low-mass systems like those under consideration here, feedback is often imagined to be driven by star formation and subsequent supernova events. In this case, we might expect some correlation between $\mathcal{E}$ and measures of star formation.

Figure 6 shows $\mathcal{E}$ as a function of past average star formation rate and gas mass fraction. The gas fraction is $f_g = M_g/M_b$; to obtain the past average star formation rate we assume all galaxies have an age of 12 Gyr so that $\langle \mathrm{SFR} \rangle = M_*/(12\ \mathrm{Gyr})$. Both of these quantities correlate with $\mathcal{E}$, albeit with substantial scatter at low $\langle \mathrm{SFR} \rangle$ and high f_g. The curious thing about these correlations is that feedback has been most effective in removing or suppressing baryons in galaxies that have experienced the least star formation and have the most cold gas remaining. This would seem to be the opposite of what one would expect from a picture in which intense star formation results in winds that drive out baryons.

The effect is not subtle. Galaxies with $f_g \approx 0.9$ have $\mathcal{E} \approx 25$; those with $\langle \mathrm{SFR} \rangle \approx 10^{-3}\ M_\odot\ \mathrm{yr}^{-1}$ have $\mathcal{E} \approx 40$. It appears that the vast majority of baryons associated with the halos of these galaxies have been ejected or otherwise suppressed.

A more remarkable thing is that $\mathcal{E}$ scales so precisely with V_f. In order not to impart scatter to the BTFR, there must be very little scatter in Equation (17). I would expect feedback from

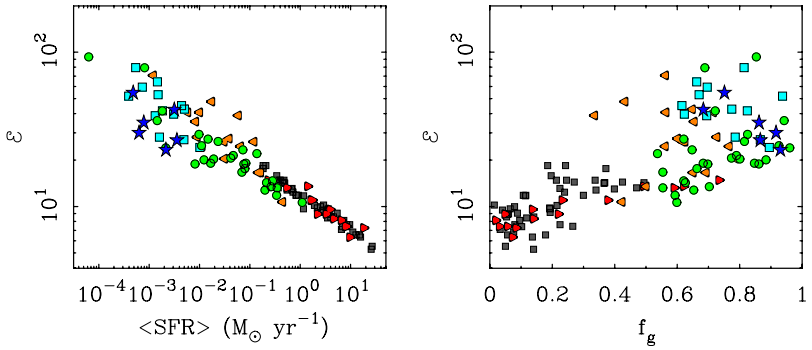

Figure 6. Efficacy of feedback (Equation (16)) as a function of past average star formation rate (left) and gas fraction (right). Symbols as per Figure 1. Feedback solutions reconciling ΛCDM with the BTFR require galaxies that have experienced the least star formation to have been most effective in driving out baryons. This holds even in galaxies where there are almost no stars ($f_g \to 1$).

(A color version of this figure is available in the online journal.)

supernovae to be a chaotic process: The lack of scatter in $\mathcal{E}$ seems unnatural. A halo of a given circular velocity could easily host galaxies of very different $\mathcal{E}$. Apparently, they do not—all halos of the same V_f have basically the same $\mathcal{E}$.

The tight relation between V_f and $\mathcal{E}$ provides strong constraints on models of galaxy formation. Indeed, it seems to me that it constitutes a serious fine-tuning problem. One can readily envision models that obtain Equation (17) as a mean scaling relation (e.g., Stringer et al. 2011). However, doing so with so little scatter is a much tougher requirement. I would expect f_d and f_V to fill out some distribution of values (e.g., Kauffmann et al. 1999; Bullock et al. 2001), even for halos of fixed mass. There is no obvious reason why these distributions should be either narrow or closely coupled. Yet they must be in order to avoid introducing substantial scatter into the BTFR.

Stochastic feedback is not the only expected source of scatter in the BTFR. The scatter in the concentration–circular velocity relation for dark matter halos is another. Without some tuning (Bullock et al. 2001), this alone exceeds the scatter allowed by the error budget.

Another expected source of scatter is the triaxiality of dark matter halos (e.g., Kazantzidis et al. 2010). If the gravitational potential is non-symmetric, then the observed velocity depends on the viewing angle with respect to the principle axis of the potential. Otherwise identical galaxies will appear to have difference V_f depending on how they happen to be oriented on the sky. A significant degree of non-axisymmetry is clearly excluded (Andersen et al. 2001; Trachternach et al. 2009; Kuzio de Naray et al. 2009). This constraint might be lessened by the rounding of dark matter halos by the formation of the baryonic disk, but the disk needs to be heavy enough to have an impact. Kazantzidis et al. (2010) find that disks need to be at least half-maximal to have a significant impact on their halos. The low surface brightness disks that make up the majority of the gas-rich galaxy sample typically fall a factor of two below this level (McGaugh 2005b).

There are other factors though could, and probably should, contribute to the scatter (Eisenstein & Loeb 1996; McGaugh & de Blok 1998a). It is difficult to accommodate all the expected sources of scatter in the error budget. This holds even if we have *overestimated* the observational uncertainties, simply because the observed scatter is small.

The small intrinsic scatter in the BTFR appears to be a serious challenge for ΛCDM. This is hardly the only problem faced by the theory (e.g., Kroupa et al. 2010; Kuzio de Naray & Spekkens 2011; Bovill & Ricotti 2011), so the persistent failure to detect weakly interacting massive particles (WIMPs) is worrisome. The XENON100 Collaboration (2011) has excluded much of the mass–cross-section parameter space where WIMPs were expected to reside (Trotta et al. 2008). Given the persistence of dynamical puzzles (e.g., McGaugh & de Blok 1998a; Sellwood & Kosowsky 2001), one might worry that non-baryonic dark matter does not exist after all.

3.1.2. Some Specific Models

The generic constraints discussed in the previous section may or may not be adequately addressed by specific models. There are very many relevant models in the literature. It is well beyond the scope of this paper to review all of them. Nevertheless, it is useful to examine several illustrative cases.

Mo et al. (1998) built a model following the same logic outlined above. They define a parameter m_d that is the fraction of the total mass in the disk. This is analogous to f_d, such that $m_d = f_b$ when $f_d = 1$. The resulting Tully–Fisher relation (their Equation (4)) is shown as lines in the first panel of Figure 5 for $m_d = 0.05$ (as they suggest) and for $m_d = 0.01$ (as suggested by Gurovich et al. 2010). The higher value gives a tolerable approximation to high-mass spirals while the lower value is appropriate to gas-dominated dwarfs. A single universal value, as often assumed in galaxy formation modeling, does not work simply because the slope of the BTFR is steeper than the ΛCDM halo-mass–rotation-velocity relation.

More recent models include semi-analytic treatments (e.g., Tonini et al. 2010; Trujillo-Gomez et al. 2011) and fully numerical results (e.g., Mayer & Moore 2004; Governato et al. 2007, 2010; de Rossi et al. 2010; Piontek & Steinmetz 2011). These are shown in the remaining panels of Figure 5. All invoke feedback in some way, but the prescription for feedback is specific to each so some come closer to match the constraint on $\mathcal{E}$ than others.

The model of Tonini et al. (2010) exhibits a substantial scatter and dependence on the distribution of stellar mass. This is natural: The distribution of baryonic mass should matter (McGaugh & de Blok 1998a). This model matches the high-mass end of the observed BTFR reasonably well, but overpredicts the mass in galaxies with $V_f \approx 100$ km s^{-1}. Nevertheless, this model, like that of Mo et al. (1998), provides an honest example of what we most naturally expect from ΛCDM: A substantial amount of scatter about a relation with a slope of approximately 3.

The model of Tonini et al. (2010) also indicates a shift in normalization of the relation for galaxies residing in sub-halos

relative to that of primary galaxies (their Figure 6). This shift is already apparent at relatively large $V_f \gtrsim 100$ km s^{-1}. There is no evidence of this in the data, which includes both primary galaxies and dwarfs that are sometimes isolated and sometimes group members (and hence sub-halos). For example, KK98-251 is a dwarf irregular satellite of NGC 6946, but both lie on the same BTFR with no indication of a shift in normalization. Current data for the ultrafaint dwarf satellites of the Milky Way do place them below the BTFR, but this shift occurs at much smaller scales ($V_f \lesssim 20$ km s^{-1}; Walker et al. 2009; Wolf et al. 2010; McGaugh & Wolf 2010).

The model of Trujillo-Gomez et al. (2011) exhibits significant curvature. It matches the data well at $V_f \sim 100$ km s^{-1} but falls below it at both high and low V_f. There is no evidence in the data for curvature in the BTFR of rotating galaxies. It is of course conceivable that curvature may appear beyond the bounds of the current data, and may already be observed if one considers dwarf spheroidals along with dwarf irregulars (McGaugh & Wolf 2010). This occurs at a significantly lower velocity scale ($\sim$20 km s^{-1}) than in the model of Trujillo-Gomez et al. (2011; $\sim$70 km s^{-1}).

The model of de Rossi et al. (2010) fares better, being in rather good agreement with the bulk of the data for gas-rich galaxies. Like most ΛCDM models, its slope is relatively shallow ($\sim$3.2; their Table 3), but this is only problematic at the high-mass end where the model underpredicts the mass of star-dominated galaxies. This might be remedied by adopting a different IMF, but the change would have to be substantial: a factor of three or so in stellar mass. The scatter is respectably small.

Most recently, detailed numerical simulations have produced model galaxies consistent with the BTFR (Governato et al. 2010; Piontek & Steinmetz 2011). These are shown in the final panel of Figure 5. Here we plot the velocity measured at the peak of the baryonic rotation curve V_p rather than V_f because this is closer to what is reported by Piontek & Steinmetz (2011). Even though there is not a great deal of difference between these two measures of rotation velocity, the already good agreement between the models and the data shown by Piontek & Steinmetz (2011) improves even further when V_p is utilized.

Numerical simulations of this sort remain computationally expensive. Piontek & Steinmetz (2011) present eight model galaxies, which at present is a large number for such models Governato et al. (2007). Of these eight, seven are very nicely consistent with the observed BTFR. As they discuss, the other case is very discrepant. Obviously, no conclusions can be drawn from one case in eight. But it does raise some obvious and important questions. What is the intrinsic scatter of the BTFR? How often we should expect to see grossly discrepant cases? Would we recognize these objects as normal disk galaxies?

Resolution also remains an issue in numerical modeling. The model galaxies of Piontek & Steinmetz (2011) are all in the star-dominated regime. Only the one model galaxy of Governato et al. (2010) resides in the regime of gas-dominated galaxies where the comparison is most clean. Comparison with the Millennium simulation suggests that simulated galaxies might well follow the observed slope and normalization of the BTFR down to low rotation velocities (S. D. M. White & Q. Guo 2011, private communication). The critical issue of the intrinsic scatter that should be exhibited by low-mass model galaxies in such simulations remains open.

Detailed numerical simulations appear to have finally reached the point where they can produce quantitatively realistic model galaxies. This is clearly a great success. It remains to be seen if they can provide a satisfactory explanation for the small intrinsic scatter in the BTFR. If they can, then the question becomes whether feedback prescriptions that accomplish this feat correspond to how feedback works in nature.

3.2. MOND

Among alternatives to dark matter, one, MOND (Milgrom 1983), makes strong a priori predictions about the BTFR, which is a consequence of the form of the force law in MOND. This deviates from purely Newtonian at small accelerations, $a \lesssim a_0$, where a_0 is the one new parameter introduced by the theory. The value of a_0 must be constrained by observation ($a_0 \approx 10^{-10}$ m s^{-2}; Sanders & McGaugh 2002), but once specified it is constant.

In the deep modified regime, $a \ll a_0$, the effective acceleration $a \rightarrow \sqrt{g_N a_0}$, where g_N is the Newtonian acceleration calculated for the observed baryonic mass in the usual way. For circular motion around a point source, we can equate the centripetal acceleration to this effective force to obtain

$$a_0 GM = V_f^4. \quad (18)$$

Since both a_0 and G are constants, and all mass is baryonic, one recognizes the BTFR, $M_b \propto V_f^4$.

There are several consequences of Equation (18) (Milgrom 1983). The Tully–Fisher relation is absolute, being a direct consequence of the force law. There should be no intrinsic scatter. The normalization is set by constants of nature. Contrary to the case in Newtonian dynamics, the circular velocity does not depend on the radial extent of the mass distribution, so there is no dependence on surface brightness or scale length. This naturally explains the lack of observed size or surface brightness residuals from the Tully–Fisher relation (Zwaan et al. 1995; Sprayberry et al. 1995; Courteau & Rix 1999; McGaugh 2005a).

Indeed, Milgrom (1983) specifically predicted that low surface brightness galaxies would share the same Tully–Fisher relation, with the same normalization, as high surface brightness spirals. This prediction was subsequently confirmed (McGaugh & de Blok 1998b). The data for gas-rich galaxies now provide the opportunity to test another a priori prediction.

3.2.1. A Test with No Free Parameters

The circular velocities of the gas-rich dwarfs considered here are measured. Their baryonic masses are observed. Their location on the BTFR is fixed. Consequently, the gas-rich dwarfs provide a test of the MOND prediction with *zero* free parameters.

The results of this test is shown in Figure 7. Even though the value of a_0 was set by early fits to bright spirals ($a_0 = 1.2$ Å s^{-2}; Begeman et al. 1991), Equation (18) fits the data for much lower mass galaxies well. The gas-rich dwarfs follow the prediction of MOND with no fitting whatsoever (McGaugh 2011).

There was no guarantee that MOND would pass the test posed by gas-rich galaxies. A Tully–Fisher-type relation is built into the MOND force law, but its slope is fixed and its normalization is constrained by star-dominated galaxies. The data for gas-rich galaxies could have fallen anywhere in the BTFR plane. They might have exhibited the slope of 3 that is more natural to ΛCDM. Instead, they fall along the one and only line permitted in MOND.

3.2.2. The Value of a_0

The data for gas-rich galaxies are consistent with existing estimates of the acceleration constant a_0 (Sanders & McGaugh

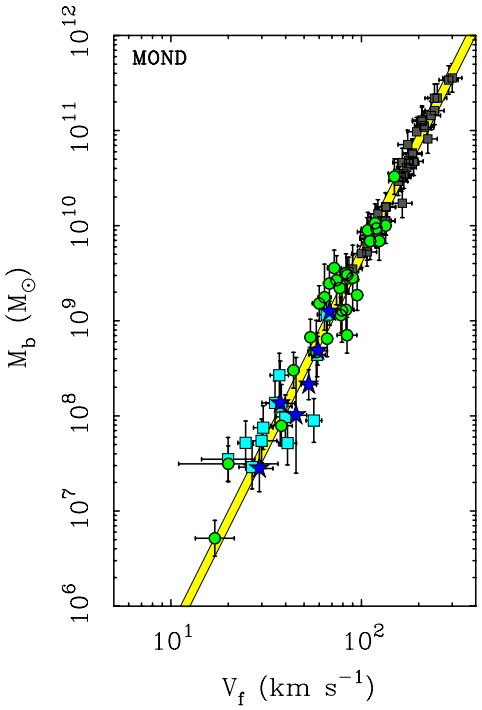

Figure 7. BTFR in MOND. Symbols as per Figure 1. The band shows the expectation of MOND (Milgrom 1983). The width of the band represents the $\pm 1\sigma$ uncertainty in a_0 based on detailed fits to the rotation curves of a subset (Begeman et al. 1991) of the star-dominated galaxies (gray squares). The gas-rich galaxies test the MOND prediction in a new regime with zero free parameters.

(A color version of this figure is available in the online journal.)

2002). We can reverse the question and ask what the best value of a_0 is according to these data. The best-fit intercept of the BTFR already contains this information, and the corresponding value of a_0 is given in Table 2.

There are some subtle issues to consider in calibrating a_0. This has previously been done by fits to full rotation curves (e.g., Begeman et al. 1991; Swaters et al. 2010). These contain more information than simply the outer circular velocity, but require an additional assumption. In particular, a form for the function that interpolates between the Newtonian and MOND regimes must be assumed. For an assumed form, the best-fit mass-to-light ratio must be found simultaneously with the best-fit value of a_0. There is not much range allowed in either of these parameters, but there can be covariance between them, so it is challenging to disentangle them uniquely. Here, the data are not so precise, and we make no use of the information in the shape of the rotation curve, only its outer value. However, this approach has the virtue of making a minimum of assumptions and using mass estimates that are completely independent of the theory.

Strictly speaking, Equation (18) applies at infinite distance from an isolated point mass. Real galaxies are not point masses, and V_f is measured at a finite radius. Consequently, the intercept of the empirical BTFR is related to the acceleration constant of MOND by

$$A = \frac{\chi}{a_0 G}, \tag{19}$$

where χ is a factor of order unity that accounts for the finite size and non-spherical geometry of galaxies.

McGaugh & de Blok (1998b) estimated $\chi = 0.76$ from purely geometrical considerations—thin disks rotate faster than the equivalent spherical mass distribution. The sample discussed by McGaugh (2005b) has MOND fits performed for $a_0 = 1.2$ Å s^{-2} and a separate fit for the BTFR yielding $A = 50\, M_\odot$ km^{-4} s^4. This gives an empirical estimate of $\chi = 0.80$, which I adopt here. The gas-rich galaxy data thus give

$$a_0 = 1.3 \pm 0.3 \text{ Å s}^{-2}. \tag{20}$$

The uncertainty here includes the formal uncertainty in A (Equation (9)) plus an allowance for 20% uncertainty in χ. It is conceivable that there could be a small systematic offset in the mean value of χ between gas- and star-dominated galaxies.

Detailed rotation curve fits to some of the same galaxies suggest $a_0 \approx 0.7$ Å s^{-2} (Swaters et al. 2010). This becomes $a_0 \approx 1.0$ Å s^{-2} if we exercise the same quality control on the data as applied here. This gives some idea of the systematic uncertainty and the impact of the best-fit stellar mass-to-light ratio when it is treated as a fitting parameter along with a_0. However, data quality remains the paramount issue.

The BTFR is clearly a success of MOND, despite its many other drawbacks. Further tests are possible, as adherence to the BTFR does not guarantee that it is possible to obtain an acceptable fit to the entire rotation curve of each galaxy. While MOND is known to do quite well in some gas-rich galaxies (e.g., Gentile et al. 2010), it may have problems in others (e.g., Sanchez-Salcedo & Hidalgo-Gamez 2011, where again the issue appears to be with the inclination). It is particularly challenging to fit the full rotation curve of NGC 3198 (Bottema et al. 2002; Gentile et al. 2011), the most massive galaxy to meet the gas-rich criterion imposed here. Perhaps this suffices to falsify MOND, but we should not be so eager to disbelieve MOND as a theory that we ignore the remarkable empirical virtues of the simple formula suggested by Milgrom (1983).

There are other suggestions for modifying gravitational theory besides MOND. Conformal Weyl gravity (Mannheim & Kazanas 1989) and MoG (Moffat 2006) offer two examples. If these theories can fit rotation curves (Brownstein & Moffat 2006; Mannheim & O'Brien 2010), then they will also fit the BTFR (Moffat & Toth 2011). However, I am not aware of a clear a priori prediction of this phenomenon by any theory other than MOND.

4. CONCLUSIONS

The baryonic mass–velocity relation provides an important test of ΛCDM and alternatives like MOND. I have assembled recent data for gas-rich rotating galaxies in order to test these theories. With $M_g > M_*$, the location of these objects in the baryonic mass–rotation velocity plane is effectively measured directly from observations without the usual systematic uncertainty in the stellar mass-to-light ratio.

A long-standing prediction (Milgrom 1983) of MOND is that rotating galaxies will fall on a single mass–velocity relation with slope 4: $M_b \propto V_f^4$. This prediction is realized in multiple independent data sets. Gas-rich galaxies fall where predicted by MOND with no free parameters. There are not many predictions in extragalactic astronomy that fare so well over a quarter century after their publication.

In ΛCDM, the naive expectation of a Tully–Fisher-type relation with a slope around 3 fails to predict the location of gas-rich galaxies in the plane of the BTFR. Only the most recent detailed numerical models (e.g., Governato et al. 2010; Piontek & Steinmetz 2011) succeed in reproducing the observed phenomenology. This is certainly progress. However, a physical

understanding for why galaxy formation in the context of ΛCDM should pick out the particular phenomenology predicted a priori by MOND is needed.

The work of S.S.M. is supported in part by NSF grant AST 0908370.

REFERENCES

Andersen, D. R., Bershady, M. A., Sparke, L. S., Gallagher, J. S., III, & Wilcots, E. M. 2001, ApJ, 551, L131
Anderson, M. E., & Bregman, J. N. 2010, ApJ, 714, 320
Begeman, K. G., Broeils, A. H., & Sanders, R. H. 1991, MNRAS, 249, 523
Begum, A., Chengalur, J. N., Karachentsev, I. D., & Sharina, M. E. 2008a, MNRAS, 386, 138
Begum, A., Chengalur, J. N., Karachentsev, I. D., Sharina, M. E., & Kaisin, S. S. 2008b, MNRAS, 386, 1667
Bell, E. F., & de Jong, R. S. 2001, ApJ, 550, 212
Bell, E. F., McIntosh, D. H., Katz, N., & Weinberg, M. D. 2003, ApJS, 149, 289
Bothun, G. D., Aaronson, M., Schommer, B., et al. 1985, ApJS, 57, 423
Bottema, R., Pestaña, J. L. G., Rothberg, B., & Sanders, R. H. 2002, A&A, 393, 453
Bovill, M. S., & Ricotti, M. 2011, ApJ, 741, 18
Brownstein, J. R., & Moffat, J. W. 2006, ApJ, 636, 721
Bullock, J. S., Kolatt, T. S., Sigad, Y., et al. 2001, MNRAS, 321, 559
Conroy, C., Gunn, J. E., & White, M. 2009, ApJ, 699, 486
Courteau, S., Dutton, A. A., van den Bosch, F. C., et al. 2007, ApJ, 671, 203
Courteau, S., & Rix, H. 1999, ApJ, 513, 561
Dalcanton, J. J., & Stilp, A. M. 2010, ApJ, 721, 547
Das, M., Boone, F., & Viallefond, F. 2010, A&A, 523, A63
Das, M., O'Neil, K., Vogel, S. N., & McGaugh, S. 2006, ApJ, 651, 853
de Blok, W. J. G., & McGaugh, S. S. 1998, ApJ, 508, 132
de Blok, W. J. G., McGaugh, S. S., & van der Hulst, J. M. 1996, MNRAS, 283, 18
de Blok, W. J. G., Walter, F., Brinks, E., et al. 2008, AJ, 136, 2648
de Rossi, M. E., Tissera, P. B., & Pedrosa, S. E. 2010, A&A, 519, A89
Eder, J. A., & Schombert, J. M. 2000, ApJS, 131, 47
Eisenstein, D. J., & Loeb, A. 1996, ApJ, 459, 432
Eke, V. R., Navarro, J. F., & Steinmetz, M. 2001, ApJ, 554, 114
Franx, M., & de Zeeuw, T. 1992, ApJ, 392, L47
Freedman, W. L., Madore, B. F., Gibson, B. K., et al. 2001, ApJ, 553, 47
Freeman, K. C. 1999, in ASP Conf. Ser. 170, The Low Surface Brightness Universe, ed. J. I. Davies, C. Impey, & S. Phillips (San Francisco, CA: ASP), 3
Gentile, G., Baes, M., Famaey, B., & van Acoleyen, K. 2010, MNRAS, 406, 2493
Gentile, G., Famaey, B., & de Blok, W. J. G. 2011, A&A, 527, A76
Gentile, G., Salucci, P., Klein, U., & Granato, G. L. 2007, MNRAS, 375, 199
Gnedin, O. Y., Weinberg, D. H., Pizagno, J., Prada, F., & Rix, H. 2007, ApJ, 671, 1115
Governato, F., Brook, C., Mayer, L., et al. 2010, Nature, 463, 203
Governato, F., Willman, B., Mayer, L., et al. 2007, MNRAS, 374, 1479
Gurovich, S., Freeman, K., Jerjen, H., Staveley-Smith, L., & Puerari, I. 2010, AJ, 140, 663
Gurovich, S., McGaugh, S. S., Freeman, K. C., et al. 2004, PASA, 21, 412
Helfer, T. T., Thornley, M. D., Regan, M. W., et al. 2003, ApJS, 145, 259
Isobe, T., Feigelson, E. D., Akritas, M. G., & Babu, G. J. 1990, ApJ, 364, 104
Kauffmann, G., Colberg, J. M., Diaferio, A., & White, S. D. M. 1999, MNRAS, 303, 188
Kazantzidis, S., Abadi, M. G., & Navarro, J. F. 2010, ApJ, 720, L62
Komatsu, E., Dunkley, J., Nolta, M. R., et al. 2009, ApJS, 180, 330
Kroupa, P. 2002, Science, 295, 82
Kroupa, P., Famaey, B., de Boer, K. S., et al. 2010, A&A, 523, A32
Kuzio de Naray, R., McGaugh, S. S., & Mihos, J. C. 2009, ApJ, 692, 1321
Kuzio de Naray, R., & Spekkens, K. 2011, ApJ, 741, L29
Leroy, A. K., Walter, F., Brinks, E., et al. 2008, AJ, 136, 2782
Mannheim, P. D., & Kazanas, D. 1989, ApJ, 342, 635
Mannheim, P. D., & O'Brien, J. G. 2010, arXiv:1011.3495
Masters, K. L., Springob, C. M., & Huchra, J. P. 2008, AJ, 135, 1738
Matthews, L. D., & Gao, Y. 2001, ApJ, 549, L191
Matthews, L. D., Gao, Y., Uson, J. M., & Combes, F. 2005, AJ, 129, 1849
Matthews, L. D., van Driel, W., & Gallagher, J. S., III. 1998, AJ, 116, 2196
Mayer, L., & Moore, B. 2004, MNRAS, 354, 477
McGaugh, S. S. 2005a, Phys. Rev. Lett., 95, 171302
McGaugh, S. S. 2005b, ApJ, 632, 859
McGaugh, S. S. 2011, Phys. Rev. Lett., 106, 121303
McGaugh, S. S., & de Blok, W. J. G. 1997, ApJ, 481, 689
McGaugh, S. S., & de Blok, W. J. G. 1998a, ApJ, 499, 41
McGaugh, S. S., & de Blok, W. J. G. 1998b, ApJ, 499, 66
McGaugh, S. S., Schombert, J. M., Bothun, G. D., & de Blok, W. J. G. 2000, ApJ, 533, L99
McGaugh, S. S., Schombert, J. M., de Blok, W. J. G., & Zagursky, M. J. 2010, ApJ, 708, L14
McGaugh, S. S., & Wolf, J. 2010, ApJ, 722, 248
Meurer, G. R., Carignan, C., Beaulieu, S. F., & Freeman, K. C. 1996, AJ, 111, 1551
Mihos, J. C., McGaugh, S. S., & de Blok, W. J. G. 1997, ApJ, 477, L79
Milgrom, M. 1983, ApJ, 270, 371
Mo, H. J., & Mao, S. 2004, MNRAS, 353, 829
Mo, H. J., Mao, S., & White, S. D. M. 1998, MNRAS, 295, 319
Moffat, J. W. 2006, J. Cosmol. Astropart. Phys., 3, 4
Moffat, J. W., & Toth, V. T. 2011, arXiv:1103.5634
Noordermeer, E., & Verheijen, M. A. W. 2007, MNRAS, 381, 1463
Oh, S., de Blok, W. J. G., Walter, F., Brinks, E., & Kennicutt, R. C. 2008, AJ, 136, 2761
O'Neil, K., Hofner, P., & Schinnerer, E. 2000, ApJ, 545, L99
O'Neil, K., & Schinnerer, E. 2004, ApJ, 615, L109
Persic, M., & Salucci, P. 1991a, MNRAS, 248, 325
Persic, M., & Salucci, P. 1991b, ApJ, 368, 60
Pfenniger, D., Combes, F., & Martinet, L. 1994, A&A, 285, 79
Pfenniger, D., & Revaz, Y. 2005, A&A, 431, 511
Piontek, F., & Steinmetz, M. 2011, MNRAS, 410, 2625
Portinari, L., Sommer-Larsen, J., & Tantalo, R. 2004, MNRAS, 347, 691
Reyes, R., Mandelbaum, R., Gunn, J. E., et al. 2011, arXiv:1110.4107
Sakai, S., Mould, J. R., Hughes, S. M. G., et al. 2000, ApJ, 529, 698
Sanchez-Salcedo, F. J., & Hidalgo-Gamez, A. M. 2011, arXiv:1105.2612
Sanders, R. H. 1984, A&A, 136, L21
Sanders, R. H., & McGaugh, S. S. 2002, ARA&A, 40, 263
Schombert, J. M., Pildis, R. A., & Eder, J. A. 1997, ApJS, 111, 233
Sellwood, J. A., & Kosowsky, A. 2001, in ASP Conf. 240, Gas and Galaxy Evolution, ed. J. E. Hibbard, M. Rupen, & J. H. van Gorkom (San Francisco, CA: ASP), 311
Sellwood, J. A., & McGaugh, S. S. 2005, ApJ, 634, 70
Sprayberry, D., Bernstein, G. M., Impey, C. D., & Bothun, G. D. 1995, ApJ, 438, 72
Stark, D. V., McGaugh, S. S., & Swaters, R. A. 2009, AJ, 138, 392
Steinmetz, M., & Navarro, J. F. 1999, ApJ, 513, 555
Stringer, M. J., Bower, R. G., Cole, S., Frenk, C. S., & Theuns, T. 2011, arXiv:1111.2529
Swaters, R. A., Sancisi, R., van Albada, T. S., & van der Hulst, J. M. 2009, A&A, 493, 871
Swaters, R. A., Sanders, R. H., & McGaugh, S. S. 2010, ApJ, 718, 380
Tikhonov, A. V., & Klypin, A. 2009, MNRAS, 395, 1915
Tonini, C., Maraston, C., Ziegler, B., et al. 2010, MNRAS, 415, 811
Torres-Flores, S., Epinat, B., Amram, P., Plana, H., & Mendes de Oliveira, C. 2011, MNRAS, 416, 1936
Trachternach, C., de Blok, W. J. G., McGaugh, S. S., van der Hulst, J. M., & Dettmar, R. 2009, A&A, 505, 577
Trotta, R., Feroz, F., Hobson, M., Roszkowski, L., & Ruiz de Austri, R. 2008, J. High Energy Phys., JHEP12(2009)024
Trujillo-Gomez, S., Klypin, A., Primack, J., & Romanowsky, A. J. 2011, ApJ, 742, 16
Tully, R. B., & Fisher, J. R. 1977, A&A, 54, 661
Tully, R. B., & Fouque, P. 1985, ApJS, 58, 67
Tully, R. B., Pierce, M. J., Huang, J., et al. 1998, AJ, 115, 2264
Tully, R. B., & Verheijen, M. A. W. 1997, ApJ, 484, 145
van den Bosch, F. C. 2000, ApJ, 530, 177
Verheijen, M. A. W. 2001, ApJ, 563, 694
Walker, M. G., Mateo, M., Olszewski, E. W., et al. 2009, ApJ, 704, 1274
Walter, F., Brinks, E., de Blok, W. J. G., et al. 2008, AJ, 136, 2563
Weiner, B. J., Willmer, C. N. A., Faber, S. M., et al. 2006, ApJ, 653, 1049
Wolf, J., Martinez, G. D., Bullock, J. S., et al. 2010, MNRAS, 406, 1220
XENON100 Collaboration. 2011, Phys. Rev. Lett., 107, 131302
Yegorova, I. A., & Salucci, P. 2007, MNRAS, 377, 507
Young, J. S., & Knezek, P. M. 1989, ApJ, 347, L55
Zwaan, M. A., van der Hulst, J. M., de Blok, W. J. G., & McGaugh, S. S. 1995, MNRAS, 273, L35